A Near-Infrared Imaging Survey of the Chamaeleon I Dark Cloud

Mercedes Gómez[1]

Observatorio Astronómico de Córdoba, Laprida 854, 5000 Córdoba, Argentina

mercedes@oac.uncor.edu

and

Scott J. Kenyon[1]

Smithsonian Astrophysical Observatory, 60 Garden Street, Cambridge MA 02138

skenyon@cfa.harvard.edu

Received ______________; accepted ______________

Submitted to AJ

[1]Visiting Astronomer, Cerro Tololo Inter-American Observatory. CTIO is operated by AURA, Inc. under contract to the National Science Foundation.

ABSTRACT

We describe a near-infrared imaging survey covering $\sim$ 1 deg^2 of the Chamaeleon I dark cloud. The survey is complete for K < 15.0, H < 16.0, and J < 16.5, roughly two magnitudes more sensitive than previous large scale surveys. We use the large number of background stars detected to derive an accurate near-infrared extinction law for the cloud and select new candidate members with near-infrared color excesses. We list $\sim$ 100 candidates of the cloud with K $\geq$ 12.0, based on their positions in the $J-H$, $H-K$ color-color diagram. These new stars have low luminosities ($K \sim 12$ – 16, $H-K \gtrsim 0.5$ – 1.5) and may have masses close to or even below the hydrogen burning limit.

Subject headings: ISM: individual (Chamaeleon I) — ISM: dust, extinction — star: formation — stars: low-mass stars, brown dwarfs — star: pre-main sequence

1. Introduction

The Chamaeleon I dark cloud ($\alpha \sim 11^{\rm h}$, $\delta \sim -77^{\rm o}$) is an active stellar nursery with 150 or more known young stars (Schwartz 1991; Gauvin and Strom 1992; Lawson et al. 1996; Cambrésy et al. 1998; Comerón et al. 1999). Located at a distance of $\sim$ 160 pc (Whittet et al. 1997), it has a relatively small angular size (Boulanger et al. 1998, $\sim$ 3 deg^2). Because of its proximity and moderate extension on the sky the Chamaeleon I star-forming region is an attractive place to attempt to measure the initial mass function (IMF), particularly at low masses (i.e., for masses $\leq$ 0.1 $M_\odot$).

Here we report results of a JHK imaging survey of the Cha I dark cloud, which covers an area of $\sim$ 1 deg^2 and is complete for K < 15.0, H < 16.0, and J < 16.5. Our survey complements the IJK_s observations of DENIS (Deep Near Infrared Southern Sky Survey, ESO, 1m tel, Epchtein (1997)) described by Cambrésy et al. (1998). The DENIS survey covers a larger area, $1.5^o \times 3^o$, of the cloud; but, with a sensitivity of $K_s < 13.5$, it is less sensitive to the lowest mass cloud members. Cambrésy et al. (1998) proposed 54 new candidate young stars, based on their locations in the $I-J/J-K$ diagram. In addition our survey area comprises two areas, in the the northern region, recently observed by Persi et al. (1999) and Oasa et al. (1999). The data reported by these authors are ~ 2 magnitudes deeper than ours but cover modest areas on the cloud ($\sim 3' \times 3'$, Persi et al. (1999); $\sim 6' \times 6'$, Oasa et al. (1999)) centered close to the high-velocity $C^{18}O$ bipolar outflow previously detected by Mattila (1989). Persi et al. (1999) identified a new Class I source of the cloud. Oasa et al. (1999) proposed 9 new very low luminosity members of the cloud.

Our survey recovers 40 of these DENIS candidates (lying on common areas to both surveys) and the stars with $K < 15.5$ detected by Persi et al. (1999) and Oasa et al. (1999). In addition the present observation yields ~ 100 new candidates with $K \geq 12$ and near-infrared excess emission in the $J-H$,$H-K$ color-color diagram. The low luminosities of these candidates suggests they may be very low mass cloud members, with masses close to or below the hydrogen burning limit.

We describe our observations, data reduction, and analysis in §2. The astrometry and photometry were obtained for $\sim$ 11,090 sources at JHK detected in our survey region. In §3 we derive a reliable extinction curve for background stars and use this curve to propose ~ 100 new potential young stellar objects based on their location in the $J-H/H-K$ diagram in §4. We conclude with a brief summary in §5.

2. Observations and Data Analysis

We obtained JHK imaging data for the Chamaeleon I dark cloud and three relatively unreddened control fields on 13–16 February 1995, 8–11 March 1996, 16–19 April 1997, and 1–2 November 1998 with CIRIM (the Cerro Tololo Infrared Imager) at the CTIO 1.5m telescope. The CIRIM uses a 256 × 256 HgCdTe NICMOS 3 array, which provides a field of $\sim 4.9' \times 4.9'$ with a plate scale of $1.16''$ per pixel. We covered an area of $\sim 0.65^o \times 1.5^o$ on the cloud on a rectangular grid, with $1'$ overlap between adjacent frames. We acquired two 6 × 5 sec exposures for each field, shifted by $20''$. Figure 1 shows the extent of the survey relative to the H_2CO contour map measured by Toriseva and Mattila (1985) and the distribution of previously known young members of the cloud (Schwartz 1991; Gauvin and Strom 1992; Lawson et al. 1996; Cambrésy et al. 1998; Comerón et al. 1999). Cha I has a remarkable low-mass star formation activity localized mainly in three groups. These small clusters are situated near three reflection nebulae: Ced 112 (HD 97300), Ced 110, and Ced 111 (HD 97048), from North to South.

Our three control fields, covering an area of ~ 0.05 deg^2 and selected from a visual inspection of the ESO Red Sky Survey prints, are close to the survey region and relatively free from significant optical extinction. These off-cloud regions lie outside the limits of Figure 1, $\sim$ 1.5–2 deg away from the H_2CO boundaries, one to the North and the other two to the East and West, respectively. Table 1 gives positions and total areas covered by each of the off-cloud regions.

We processed the data using standard techniques with the software package IRAF[2].

[2]IRAF is distributed by the National Optical Astronomy Observatory, which is operated by the Association of Universities for Research in Astronomy, Inc. under contract to the National Science Foundation.

From each program frame, we subtracted an average dark frame, divided by a normalized flat-field frame appropriate for each filter, and then subtracted a flattened sky frame. The dark frame is the average of ~ 40 individual dark images taken at the beginning and end of each night. We constructed flat-field frames for each night by median-filtering all 6×5 sec frames taken in each filter. We also obtained a set of " dome flats " in each filter before observing each night using an illuminated white spot in the CTIO 1.5-m dome. Flat-fields constructed from " dome flats " and " sky flats " were identical. Sky frames were generated from a median-filtered set of 20–30 flattened frames in each filter. In this case, we combined individual object frames obtained close in time and in position to the program frame.

To produce a combined image from each dithered pair of images, we aligned the frames using the IRAF subroutines GEOMAP and GEOTRAN, added the co-aligned frames together, and trimmed the resulting image to remove bad pixels at the edges of the frames. We selected the K images as the reference frames and transformed the J and H images to the same pixel scale as the K images. We used DAOFIND to locate stars 4σ above the local background and added to the DAOFIND list all stellar objects missed by this routine, found by visual inspection of each image. We then derived photometry for each image using the APPHOT PHOT task, using a circular aperture with $5''$ radius. This aperture size includes the total flux for the large majority of sources. However, in some cases, we used a smaller aperture (i.e. $2.5''$) to avoid contamination from very close stars. Several iterations of this process produced an homogeneous set of data for the complete survey. We detected $\sim$ 11,090 sources at JHK in our survey region.

To calibrate our photometry, we observed on each night a set of 10-15 standards from Elias et al. (1982) and from the UKIRT faint JHK standard stars list (Casali and Hawarden 1992). We estimate an uncertainty of $\pm$ 0.03 mag in our calibration. The standard stars were observed at a similar airmass range as our target fields. Airmass corrections for our data are smaller than our photometric uncertainties. We used common stars on dithered pairs and measurements of duplicate stars in the overlapping regions of adjacent frames to estimate photometric uncertainties for the stars in our survey region. Table 2 lists typical photometric uncertainties in each magnitude bin. These differences reach 0.3 mag for $J \sim 17$, $H \sim 16$, and $K \sim 15$. The 5σ limiting magnitudes are $K = 14.5$, $H = 15.5$, and $J = 16.0$.

To make a check on the completeness of the survey, we constructed a list of sources from the three off-cloud regions (see Table 1). Figure 2 shows the magnitude histograms of background stars as function of the JHK magnitudes, The number of stars per bin increases monotonically up to the completeness limit and then turns over. The corresponding limits in each filter are: 16.5 at J, 16.0 at H, and 15.0 at K.

To compare our photometry with results for previous surveys, we observed $\sim$ 50 stars projected on Bok globule 2 in the Coalsack (Tapia 1975). Jones et al. (1980) and Elias et al. (1983) previously reported photometry of these stars and derived a comparison between the Mt. Stromlo/AAO photometry of Jones et al. (1980) and the CIT photometric system of Elias et al. (1982). The common photometric data between Jones et al. (1980) and our survey, together with the transformations listed in Elias et al. (1983), allow us to derive a transformation between the CIRIM and CIT photometric systems. Using the Press et al. (1992) routine FITEXY, straight line fits to the common data yield:

$$\mathrm{K_{CIRIM}} = +0.03 \pm 0.02 \ + \ 0.99 \pm 0.01 \cdot \mathrm{K_{CIT}} \tag{1}$$

$$\mathrm{(J-H)_{CIRIM}} = -0.04 \pm 0.03 \ + \ 0.95 \pm 0.02 \cdot \mathrm{(J-H)_{CIT}} \tag{2}$$

$$(\mathrm{H}-\mathrm{K})_{\mathrm{CIRIM}} = -0.02 \pm 0.02 \ + \ 1.01 \pm 0.02 \cdot (\mathrm{H}-\mathrm{K})_{\mathrm{CIT}} \tag{3}$$

The quoted uncertainties in these relations are the 1σ errors from our fits to the Mt. Stromlo/AAO data and those from the Elias et al. (1983) fits, added in quadrature. The differences between the CIRIM and CIT system are negligible for K and $H-K$, in agreement with results quoted in the CIRIM manual written by R. Elston and J. Elias[3]. We thus assume that the natural CIRIM system is identical to the CIT system for K and $H-K$. Our derived color term for $J-H$ agrees with Elston & Elias; the CIRIM $J-H$ color is bluer than the CIT $J-H$ due to its different lens design. We apply the color term to our $J-H$ data and thus quote colors in the CIT system.

To derive coordinates for our survey stars, we used WCSTool[4] (Mink 1997), a suite of programs to calculate a direct transformation between the coordinates of the image (x,y) and the sky coordinates (α,δ). We measured transformation coefficients adopting matches between program stars and stars in the U.S. Naval Observatory SA1.O Catalogue[5]. These matches provided a good transformation for $\sim$ 90% of the frames. For the rest of the frames, usually corresponding to the most obscured regions, we found few or no matches between our frames and stars in the catalog. In these cases, we used stars in common with adjacent frames with good coordinates to obtain coordinates for stars on unmatched frames. When an individual source was detected in more than one filter we adopted the average coordinate.

---

[3]Available at http://www.ctio.noao.edu/instruments/ir_instruments/cirim/cirim.html

[4]Available at ftp://cfa-ftp.harvard.edu/pub/gsc/WCSTools

[5]The U.S. Naval Observatory SA1.0 Catalogue is distributed by the U.S. Naval Observatory, Washington DC.

To verify the coordinates, we measured coordinate differences between stars on adjacent frames. Many stars have two good coordinates; others have as many as four. After visually inspecting the duplicate stars and rejecting stars too close to the edges of frames, we averaged coordinates of the remaining duplicates and derived 1σ errors. Finally, we compared coordinates derived from the Digitized Sky Survey[6] (DSS) plates. We estimate an average uncertainty in our positions of $1''$. These errors are as large as $2''$ for sources in the most obscured regions of the cloud.

Having verified the quality of the coordinates and photometry for our survey, we search for pre-main sequence stars with near-infrared excess emission in the cloud using the near-infrared color-color diagram. To identify these stars, we derive a reliable extinction curve for background stars in §3 and then consider the near-infrared color-color diagram in §4.

---

[6]Based on photographic data obtained using The UK Schmidt Telescope. The UK Schmidt Telescope was operated by the Royal Observatory Edinburgh, with funding from the UK Science and Engineering Research Council, until 1988 June, and thereafter by the Anglo-Australian Observatory. Original plate material is copyright (c) the Royal Observatory Edinburgh and the Anglo-Australian Observatory. The plates were processed into the present compressed digital form with their permission. The Digitized Sky Survey was produced at the Space Telescope Science Institute under US Government grant NAG W-2166.

3. The Cha I Near-Infrared Reddening Law

To derive the near-infrared reddening law for the Cha I dark cloud, we follow Kenyon et al. (1998a), who developed a generalized photometric technique to compare the colors of reddened stars with the colors of nearby, " unreddened " comparison stars. Kenyon et al. (1998a) assume that the stellar population behind the cloud is identical to the stellar population in off-fields several degrees away. They derive the $J - H$ and $H - K$ color excesses for each on-cloud source relative to every off-cloud source and then compute the average and median color excesses for each on-cloud source. The probable error of the average color excess is the sum in quadrature of the errors of the on-cloud and off-cloud colors. For the median color excess, the probable error is the inter-quartile range. We divide the Cha I sources into a Complete Sample containing all stars with $K < 14$ and a Restricted Sample, where we remove known young stars in the cloud from the Complete Sample. The sample of known young stars includes 94 sources (lying on our survey region) from the literature (Schwartz 1991; Gauvin and Strom 1992; Lawson et al. 1996; Cambrésy et al. 1998; Comerón et al. 1999). This sample probably is not complete; however, any incompleteness does not affect our analysis significantly.

Figure 3 shows average color excesses of Cha I stars for two K $\leq$ 14 samples, the Complete Sample and the Restricted Sample. The colors have been transformed to the CIT system using equations 1–3. The color excesses are highly correlated, with a Spearman rank-order correlation coefficient of $r_s = 0.65$ for both samples. The probability for no correlation between the two color excesses is formally zero according to the Spearman rank-order test. Straight line fits to color excess measurements with $E_{H-K} \leq 2.0$ yield $E_{J-H}/E_{H-K} = 1.63 \pm 0.03$ for the Complete Sample and $E_{J-H}/E_{H-K} = 1.76 \pm 0.02$ for the Restricted Sample. We derive identical slopes using median color excesses for each source instead of the average color excesses.

Our extinction results for the Restricted Sample are identical to the Bessell and Brett (1988) near-infrared extinction law, $E_{J-H}/E_{H-K} = 1.75$ transformed to the CIT photometric system. The Cha I results differ from the near-infrared extinction law for ρ Oph, $E_{J-H}/E_{H-K} = 1.57 \pm 0.03$ (Kenyon et al. 1998a; Elias 1978, for example) at more than the 3σ level, and are inconsistent with results from the He et al. (1995) survey of luminous southern stars, $E_{J-H}/E_{H-K} = 1.47 \pm 0.06$, at roughly the 3σ level.

Results derived for the Complete Sample demonstrate that pre-main sequence stars with near-infrared excesses skew the extinction law to smaller values (see also Kenyon et al. (1998a) and references therein). Figure 3 shows many previously identified sources with apparent near-infrared excesses. These sources probably skew our results for the reddening law derived from the Restricted Sample, although this effect should be small. Kenyon et al. (1998a) described a method, using the " reddening probability distribution ", to correct the reddening law for previously unidentified pre-main sequence stars and to derive a sample of candidate pre-main sequence stars with near-infrared excess emission. We now apply this method to the Restricted Sample of Cha I sources.

Kenyon et al. (1998a) defined the reddening probability distribution, $\rho(E_x, E_y)$, as the probability of measuring a pair of color excesses, E_x and E_y, where x and y are color indices and $N = \int \rho(E_x, E_y)\ dE_x dE_y$ is the number of reddening measurements. The number, N, is also the number of on-field stars in the sample. The density function, $\rho(E_x, E_y)$, depends on the distributions of colors in the on-field and the off-field. If $\rho_{off}(x, y)$ is the off-field color distribution and $\rho_{on}(x, y)$ as the on-field color distribution, the reddening probability distribution is:

$$\rho_{i,j}(E_x, E_y) = \sum_{k_1=1}^{N_1} \sum_{k_2=k_{min}}^{k_{max}} \ \rho_{k_1,k_2,off}(x, y)\ \rho_{k_3,k_4,on}(x, y) \tag{4}$$

where $k_3 = i + k_1 - i_0$ and $k_4 = j + k_2 - j_0$. The integers i_0 and j_0 measure the zero point offsets of the color grids; indices i and j span the full range of color indices x and y. The color distributions use a the kernel density estimator:

$$\rho(x,y) = \frac{1}{h^2}\sum_{i=1}^{N} K(x, x_i, y, y_i) \ , \tag{5}$$

where h is the smoothing parameter and K is the kernel (Silverman 1986). We follow Kenyon et al. (1998a) and adopt

$$K(\mathbf{x}) = \begin{cases} \frac{4}{\pi}(1 \ - \ \mathbf{x^T x})^3 & \text{if } \mathbf{x^T x} < 1 \\ 0 & \text{otherwise} \end{cases} \tag{6}$$

for fast computation ($\mathbf{x} = (x,\ x_i,\ y,\ y_i)$). We adopt $h = 0.2$, which is roughly twice the 1σ error of our photometry at the $K = 14$ mag survey limit. Smaller values for h produce noisy grids; larger values are inconsistent with the photometric errors.

Figure 4 shows the color distribution functions for the off-field and the Complete Sample (CS). The off-field density in the left panel has a weak maximum at the color expected for G-type giants and a sharp maximum at the color expected for K-type dwarfs. There is a plateau consistent with colors for M-type dwarfs and an extension of the dwarf locus towards the near-infrared colors of K- and M-type giant stars. The Cha I color distribution in the right panel peaks close to the off-field maximum but is much more extended. The long axis of the contours roughly follows the reddening line derived above, and there is a weak extension of sources with near-infrared excess emission at $H - K = 0.75$ and $J - H = 1.75$.

Figure 5 shows the reddening probability functions constructed from the color distributions for the Complete Sample (CS) and the Restricted Sample (RS). We derive the slope of the reddening law which follows the major axis of each contour in these diagrams using the technique outlined in (Kenyon et al. 1998a, equations 12–15). This analysis yields $E_{J-H}/E_{H-K} = 1.77 \pm 0.03$ for the Complete Sample and $E_{J-H}/E_{H-K} = 1.80 \pm 0.03$ for the Restricted Sample. These results are consistent with the reddening law derived in Figure 3 given the 1σ errors of each fit.

4. New Candidate Pre-Main Sequence Stars

Figure 6 shows the $H - K/J - H$ diagram for our complete survey region. As in Figures 3–5, we display stars with $K < 14.0$, where the photometric errors are $\lesssim 0.1$ mag. The solid line corresponds to the main sequence locus (Bessell and Brett 1988); the dashed lines, parallel to the reddening vector derived in §3, define the reddening band extending from the main sequence.

We distinguish two groups of sources in Figure 6: a) stars that lie along or follow the reddening band direction, and b) sources that show near-infrared excess, located to the right of the reddening band. The first group, comprising the majority of the sources, show negligible near-infrared color excess, and can be dereddened to lie close to the standard dwarf sequence. Most of these sources are probably behind the cloud[7]. The color excess of the second sample cannot be attributed to the reddening by dusty material in the cloud. Several authors have found that circumstellar material (disks + infalling envelopes) surrounding the young central star can produce these color excess at the near-infrared wavelengths (Lada and Adams 1992; Kenyon and Hartmann 1995). Formally speaking we have detected ~ 300 sources lying to the right of the reddening band in our survey with $K < 14.0$. Roughly 1/3 are known members of the cloud and DENIS candidates from

[7]The WTTS that belong to the cloud and that, as a class of young stellar objects, has no significant near-infrared excess may be included in this group.

Cambrésy et al. (1998). The other 2/3 are new detections. In Figure 6 we have used starred symbols to indicate new candidates with significant near-infrared excess (i.e., $H - K \gtrsim 0.5$). This group comprises ~ 50 objects. Table 3 gives coordinates and magnitudes for these stars. The rest of the sources either lie very close to the reddening line or to the bulge defined by the background stars.

Finally, our survey has also produced a list of ~ 50 faint objects (i.e., $K > 14 - 16$), with large near-infrared excess (i.e., $H - K \gtrsim 0.8$). Figure 7 shows the location of these stars in the color-color diagram. They are located well to the right of the main sequence locus. In this manner even allowing typical photometric uncertainties for these magnitudes (i.e., ~ 0.3 mag for $K \sim 15$) the sources still have color excesses. Table 4 gives coordinates and magnitudes for these stars. For these faint sources, we checked each of the images visually to avoid possible confusion with cosmic ray events, bad pixels, plate artifacts, or contamination with close stars.

A few of the objects listed in the Table 3 and Table 4 were only detected in two of the filters (K and H) and therefore J must be $\gtrsim 18.0$. These are extremely red objects and thus good candidate members of the cloud. Some of the objects display extended or fuzzy images principally at K. Four candidates were also detected by the ISOCAM survey of the Chamaeleon I dark cloud and proposed as new low-mass candidate members based on their position on the mid-infrared color-color diagram (Persi et al. 2000). We also have in common two stars with Oasa et al. (1999) (see Table 3 and Table 4).

Sources with near-infrared excess emission are either young stars in the cloud, galactic sources such as planetary nebulae (e.g., Guglielmo et al. (1998)), or galaxies. Extragalactic source counts predict 30–60 galaxies in an area similar in size to our survey region for $K \leq 14$ (e.g., Szokoly et al. (1998); Väisänen et al. (2000) and the references therein). The near-infrared extinction towards Cha I is significant (Cambrésy et al. 1997); we thus expect

$\sim$ 30% to 50% fewer galaxies in our survey compared to unobscured regions. Galaxies also tend to have smaller near-infrared excesses compared to young stars. Most galaxies have colors similar to red main sequence stars, $J-H \approx 0.6$–0.8 and $H-K \approx 0.25$–0.45, with modest near-infrared excesses of 0.2–0.3 mag in H–K (e.g., Frogel (1985); Impey et al. (1986)). Unpublished 2MASS data support this conclusion for nearby galaxies (see Jarrett et al. (1998)[8]). Our survey is not deep enough to detect more distant galaxies which could have redder near-infrared colors than measured for the nearby galaxy samples.

Several types of galactic sources, such as carbon stars and planetary nebulae, can also lie outside the reddening band in the near-infrared color-color diagram. The surface densities of these objects towards Cha I should be small, $\leq$ 5–10 deg^{-1} for carbon stars and $\leq$ 1–2 deg^{-1} for planetary nebulae (e.g., Guglielmo et al. (1998); Ortiz and Maciel (1994)).

The spatial distribution of the near-infrared excess sources provides the best evidence that these objects are pre-main sequence stars. Figure 8 compares the spatial distribution of the new candidate objects with the positions of previously known young stars (Schwartz 1991; Gauvin and Strom 1992; Lawson et al. 1996; Cambrésy et al. 1998; Comerón et al. 1999) and the H_2CO contour maps (Toriseva and Mattila 1985). The new candidates tend to cluster around Ced 112 (HD 97300), Ced 110, and Ced 111 (HD 97048) in a manner similar to the previously known members of the cloud (see Figure 1). We expect extragalactic and other galactic sources such as carbon stars and planetary nebulae to avoid regions of high obscuration and see no evidence for this tendency in our candidates.

Assuming an average inter-cloud extinction of $A_V \sim 5$ (Cambrésy et al. 1997; Cambrésy 1999, i.e., $A_K \sim 0.5$), a main-sequence star at the H burning limit and at the distance of the Cha I cloud (Whittet et al. 1997, 160 pc), would have $K \sim 15.5 - 16.0$ (Henry

[8]Available also at http://spider.ipac.caltech.edu/staff/tchester/2mass/analysis/galaxies/colors/

and McCarthy 1993). Low mass members of the Chamaeleon I dark cloud must be much younger, still contracting toward the main sequence, and thus significantly more luminous than main sequence stars of 0.1 $M_{\odot}$. Our imaging survey is complete to $K \sim 15.0$ and sensitive down to 16.5. The objects detected in this survey (with $K \sim 12 - 16$, $H - K \gtrsim 0.5 - 1.5$) are among the lowest luminosity and, presumably, lowest mass members of the cloud. Some of them are near or, probably, below the H burning limit.

Some of our candidates (with $K \sim 12 - 14$) have optical counterparts on the DSS plates. We crudely estimate V $\sim 17 - 22$ for this subgroup of candidates. Moderate resolution optical spectra would allow a search for Li I 6707 absorption, an indicator of youth, as well as other atomic (such as Hα) and many forbidden emission lines usually present in the spectra of young stellar objects (Kenyon et al. 1998b, for example). To investigate further the nature of the rest of our candidate objects we need additional 10 μm photometry and/or near-infrared spectroscopic observations. In particular, near-infrared spectra would allow us to place the stars in the HR diagram and thus, adopting recently developed pre-main sequence tracks (D'Antona and Mazzitelli 1997; Palla and Sthaler 1999, for example), determine masses and ages for the individual sources. Mass determinations are needed to estimate the lower end of the IMF. Present determinations of the IMF in the Cha I cloud are limited to 0.3 $M_{\odot}$ and for masses $\lesssim 0.6$ $M_{\odot}$ these determinations are uncertain (Appenzeller et al. 1983; Lawson et al. 1996). Age estimations will provide additional support to the concept of a coeval star-formation process in this cloud (Gauvin and Strom 1992).

5. Summary

We have used the large number of background stars detected in our survey region to derived a reliable near-infrared extinction law for the Chamaeleon I cloud. Our analysis yields E_{J-H}/E_{H-K} = 1.80 ± 0.03 for the Restricted Sample (i.e., eliminating previously known pre-main sequences stars). This result differs with the Kenyon et al. (1998a)'s determination for the ρ Oph cloud (E_{J-H}/E_{H-K} = 1.57 ± 0.03) at more than 3σ level. Based on preliminary results for other two cloud (Taurus and IC 348), in addition to their determination for ρ Oph, Kenyon et al. (1998a) suggest that a real variation in the near-infrared reddening law occurs from region to region. Our results for Cha I provide additional support for this variation.

The ratio of total to selective extinction, R_V, seems also to change for different clouds (see Kenyon et al. (1998a) and the references therein). In addition, R_V varies across the Cha I dark cloud (from $R_V \sim 3$ to $R_V \sim 5.5$; Whittet et al. (1997), see also Hyland et al. (1982)). For the ρ Oph, Vrba et al. (1993) obtained a mean value of $R_V \sim 4$, although individual determinations vary within a range similar to that found for the Cha I dark cloud. Hayakawa et al. (1999) recently found that the A_V – $N(CO)$ relation also varies among different star-forming clouds and suggest that $A_V/N(CO)$ may also change across the Chamaeleon I dark cloud. These results indicate different dust-grain properties, in particular grain-sizes, for different nearby star-forming regions and caution against using the " universal " reddening law to derive extinction estimates for young stars in star-forming regions.

Previous near-infrared observations of the cloud focussed on IRAS-selected sources (Assendorp et al. 1990; Whittet et al. 1991; Prusti et al. 1991) or already known and candidate young stellar objects detected at optical and X-ray wavelengths (Gauvin and Strom 1992; Hartigan 1993; Lawson et al. 1996; Comerón et al. 1999). These investigations were sensitive to objects with K ∼ 11 and limited to small areas around the target objects. Present imaging near-infrared surveys of the cloud have overcome these limitations (both in sensitivity and spatial coverage) and greatly increased the number of potential members of the cloud. (Persi et al. 1999) detected one new Class I source of the cloud with K $\sim$ 13. Oasa et al. (1999) proposed 9 new candidates with K = 13 – 16. (Cambrésy et al. 1998) and this paper carry out large scale near-infrared survey on the cloud. (Cambrésy et al. 1998) proposed 54 new candidates members with K $\lesssim$ 13. This paper presents an additional set of $\sim$ 100 new stars with K $\sim$ 12 – 16. In addition to these candidates selected on basis of their near-infrared color excesses, Persi et al. (2000) have recently proposed a list of 74 new low mass candidates detected by ISOCAM and selected on basis of their color excesses at the mid-infrared wavelengths.

These objects are among the lowest luminosity and, presumably, lowest mass members of the cloud. Some of them are near or, probably, below the H burning limit. A spectroscopic follow up of the optically visible candidates should provide additional indications of their pre-main sequence nature. Optical and/or near-infrared spectral types of our proposed candidates, in combination with recently developed pre-main sequence evolutionary tracks, will allow us to determine masses and ages. Reliable mass determinations are required to calculate the IMF, particular towards the sub-solar and probably into the sub-stellar mass regime. Ages determination will help to reconstruct the history of the star-formation process of the cloud.

We are grateful to the CTIO staff, specially to M. Fernández, M. Hernández, and P. Ugarte for assistance during the observing runs. We also thank R. Elston and R. Probst for their help with CIRIM, D. Mink for assistance with the WSCTools software and the anonymous referee for suggestions that improved the manuscript. This research was partially supported by the Scholarly Studies Program of the Smithsonian Institution and the National Aeronautics and Space Administration (grants: NAGW-2919 and GO-06132.01.94A). M.G. acknowledges support from the National Science Foundation through grants GF-1001-96 and GF-1001-97 from the Association of Universities for

Research in Astronomy, Inc., under NSF cooperative agreement AST-8947990.

REFERENCES

Appenzeller, I., Jankovics, I., and Krautter, J. 1983, A&A, 53, 291

Assendorp, R., Wesselius, P. R., Whittet, D. C. B., and Prusti, T. 1990, MNRAS, 247, 624

Bessell, M. S., and Brett, J. M. 1988, PASP, 100, 1134

Boulanger, F., Bronfman, L., Dame, T. M., and Thaddeus, P. 1998, A&A, 332, 273

Cambrésy, L. 1999, A&A, 345, 965

Cambrésy, L., Copet, E., Epchtein, N., de Batz, B., Borsenberger, J., Fouqué, P., Kimeswenger, S., and Tiphéne, D. 1998, A&A, 338, 977

Cambrésy, L., Epchtein, N., Copet, E., de Batz, B., Kimeswenger, S., Le Bertre, T., Rouan, D., and Tiphéne, D. 1997, A&A, 324, L5

Casali, M. M., and Hawarden, T. G. 1992, In: JCMT-UKIRT Newsletter No. 3, 33

Comerón, F., Rieke, G. H., and Neuhäuser, R. 1999, A&A, 343, 477

D'Antona, F., and Mazzitelli, I. 1997, Mem. Soc. Astron. Ital., 68, 807

Elias, J. 1978, ApJ, 224, 453

Elias, J., Fogel, J. A., Matthews, K., and Neugebauer, G. 1982, AJ, 87, 1029

Elias, J., Fogel, J. A., Hyland, A. R., and Jones, T. J. 1983, AJ, 88, 1027

Epchtein, N. 1997, In: Garzón, F., Epchtein, N., Omount, A., Burton, B., Persi, P. (eds.) The Impact of Large Scale Near-Infrared Sky Surveys, Kluwer Academic Publishers, 15

Frogel, J. A. 1985, ApJ, 298, 528

Gauvin, L. S., and Strom, K. M. 1992, ApJ, 385, 217

Guglielmo, F., Le Bertre, T., and Epchtein, N. 1998, A&A, 334, 609

Hartigan, P. 1993, AJ, 105, 1511

Hayakawa, T., Mizunon, A., Onishi, T., Yonekura, Y., Hara, A., Yamaguchi, R., and Fukui, Y. 1999, PASJ, 51, 919

He, L., Whittet, D. C. B., Kilkenny, D., and Spencer Jones, J. H. 1995, ApJS, 101, 335

Impey, C. D., Wynn-Willians, C. G., and Becklin, E. E. 1986, ApJ, 309, 572

Jarrett, H., Chester, T., Huchra, J., and Schneider, S., 1998, BAAS, 30, 900

Henry, T., and McCarthy, Jr. D. W. 1993, AJ, 106. 773

Hyland, A. R., Jones, T., and Michell, R. M. 1982, MNRAS, 201, 1095

Jones, T. J., Hyland, A. R., Robinson, G., Smith, R., and Thomas, J. 1980, ApJ, 242, 132

Kenyon, S. J., and Hartmann, L. 1995, ApJS, 101, 117

Kenyon, S. J., Brown, D. I., Tout, C. A., and Berlind, P. 1998, AJ, 115, 2359

Kenyon, S. J., Lada, E. A., and Barsony, M. 1998, AJ, 115, 252

Lada, C. J., and Adams, F. C. 1992, ApJ, 393, 278

Lawson, W. A., Feigelson, E. D., and Huenemoerder, D. P. 1996, MNRAS, 280, 1071

Mattila, K., Liljeströn, T., and Toriseva, M. 1989, In: Reipurth, B. (ed.) Low Mass Star Formation and Pre-Main Sequence Objects (Garching: ESO), 153

Mink, D. J. 1997, In: Hunt, G., Payne, H. E. (eds.) VI ASP Conf. Series, 125, Astronomical Data Analysis Software and Systems, 249

Oasa, Y., Tamura, M., and Lawson, W. A. 1999, ApJ, 526, 336

Ortiz, R., and Maciel, W. J. 1994, A&A287, 552

Palla, F., and Sthaler, S. 1999, ApJ, 525, 772

Persi, P., Marenzini, A. R., Kaas, A. A., Olofsson, G., Nordh, L., and Roth, M. 1999, AJ, 117,439

Persi, P., Marenzini, A. R., Olofsson, G., Kaas, A. A., Nordh, L., Huldtgren, M., Abergel, A., André, P., Bontemps, S., Boulanger, F., Burgdorf, M., Casali, M. M., Cesarsky, C. J., Copet, E., Davies, J., Falgarone, E., Montmerle, T., Perault, M., Prusti, T., Puget, J. L., and Sibille, F. 2000, A&A, 357, 1020

Press, W. H., Flannery, B. P., Teukolsky, S. A., Vetterling, W.T. 1992, Numerical Recipes in FORTRAN (2d ed: Cambridge: Cambridge Univ. Press).

Prusti, T., Clark, F. O., Whittet, D. C. B., Laureijis, R. J., and Zhang , C. Y. 1991, MNRAS, 251, 303

Schwartz, R. D. 1991, In: Reipurth, B. (ed.) ESO Scientific Report No. 11, Low Mass Star Formation in Southern Molecular Clouds, 93

Silverman, B. W. 1986, Density Estimator for Statistics and Data Analysis (London: Chapman & Hall)

Szokoly, G. P., Subbarao, M. U., and Connolly, A. J. 1998, ApJ, 492, 452

Tapia, S. 1975, In: Greenberg, J. M., and van de Hulst, H. C. (eds.) IAU Symposium 52, Interstellar Dust and Related Topics, 43

Toriseva, M., and Mattila, K. 1985, A&A, 153, 207

Väisänen, P., Tollestrup, E. V., and Cohen, M. 2000, ApJ, 540, 593

Vrba, F. J., Coyne, G. V., and Tapia, S. 1993, AJ, 105, 1010

Whittet, D. C. B., Prusti, T., Franco, G. A. P., Gerakines, P. A., Kilkenny, D., Larson, K., and Wesselius, P. R. 1997, A&A, 327, 1194

Whittet, D. C. B., Prusti, T., and Wesselius, P.R. 1991, MNRAS, 249, 319

Fig. 1.— The extent of our near-infrared survey relative to the H_2CO contour maps from (Toriseva and Mattila 1985) and the distribution of previously known members of the cloud (Schwartz 1991; Gauvin and Strom 1992; Lawson et al. 1996; Cambrésy et al. 1998; Comerón et al. 1999, dots). The large starred symbols indicate the positions of Ced 112 (HD 97300), Ced 110, and Ced 111 (HD 97048) from North to South, respectively.

Fig. 2.— Histogram distribution of magnitudes for background stars in our control fields. The completeness limit in each band is indicated by the dashed vertical lines.

Fig. 3.— Average color-excess diagram for two samples of the Chamaeleon I stars with K $\leq$ 14.0. The left panel shows the Complete Sample (CS) and the right panel the Restricted Sample (RS). This second sample only includes near-infrared sources not known to be pre-main sequence stars.

Fig. 4.— Color density distribution for sources in the off-field region (left panel) and for Cha I sources Complete Sample (CS, right panel).

Fig. 5.— Reddening probability distribution for the Complete Sample (CS) and the Restricted Sample (RS). The dot-dashed line indicates our best reddening law; the dashed line shows a standard reddening law with $E_{J-H}/E_{H-K} = 1.75$.

Fig. 6.— Color-color diagram for near-infrared sources with $K < 14.0$ in our survey region (see Figure 1). The solid line indicates the main sequence locus (Bessell and Brett 1988) and the two parallel lines define the reddening band, extending from the main sequence. To define this band we used the reddening vector ($E_{J-H}/E_{H-K} = 1.80 \pm 0.03$) derived for the Restricted Sample (RS in Figure 5, left panel). Typical photometric errors for $K \sim 14.0$ are displayed in the upper left corner.

Fig. 7.— Color-color diagram for near-infrared sources with $K > 14.0$ in our survey region

(see Figure 1). The solid line indicates the main sequence locus (Bessell and Brett 1988) and the two parallel lines define the reddening band, extending from the main sequence. To define this band we used the reddening vector ($E_{J-H}/E_{H-K} = 1.80 \pm 0.03$) derived for the Restricted Sample (RS in Figure 5, left panel). Typical photometric errors for $K \sim 15.0$ are displayed in the upper left corner.

Fig. 8.— Spatial Distribution of the new candidate young stellar objects (triangles) listed in the Table 3 and Table 4 in relation to the H_2CO contour maps (Toriseva and Mattila 1985) and the previously known members of the cloud (Schwartz 1991; Gauvin and Strom 1992; Lawson et al. 1996; Cambrésy et al. 1998; Comerón et al. 1999, dots). The large starred symbols indicate the position of Ced 112 (HD 97300), Ced 110, and Ced 111 (HD 97048) from North to South, respectively.

Table 1. Off-Cloud Regions.

Region	$\alpha(2000.0)$	$\delta(2000.0)$	Area
I	11 31 43	−77 38 22	$5' \times 5'$
II	10 41 24	−77 38 35	$10' \times 10'$
III	11 16 52	−77 08 42	$5' \times 10'$

Note. — Units of right ascension are hours, minutes, and seconds, and units of declination are degrees, arcminutes, and arcseconds.

Table 2. Mean Photometric Errors.

Mag. Bin	K	H	J
8 – 9	0.02	0.01	0.01
9 – 10	0.03	0.02	0.02
10 – 11	0.03	0.02	0.02
11 – 12	0.03	0.03	0.03
12 – 13	0.04	0.03	0.03
13 – 14	0.07	0.04	0.03
14 – 15	0.12	0.08	0.05
15 – 16	0.26	0.12	0.07
16 – 17	0.46	0.20	0.09
17 – 18	···	0.38	0.15

Table 3. Candidate Pre-Main Sequence Stars with $K < 14.0$.

Star	α(2000.0)	δ(2000.0)	K	$H - K$	$J - H$	Id.	Ref.
1	11 04 34.0	−78 01 26	13.34	0.68	1.00		
2	11 04 41.5	−77 38 52	13.64	0.73	1.09		
3	11 04 49.2	−78 04 46	12.48	0.75	1.03		
4	11 04 59.5	−77 17 00	12.59	0.85	0.84		
5	11 05 27.2	−77 33 09	11.80	2.99	1.24		
6	11 05 43.0	−77 29 13	13.79	1.34	1.74		
7	11 05 43.4	−77 21 22	13.81	0.83	0.85		
8	11 05 48.8	−76 40 17	13.94	0.73	0.55		
9	11 05 57.8	−76 40 56	13.06	0.84	0.79		
10	11 06 08.8	−76 56 02	13.56	0.73	0.91		
11	11 06 18.6	−77 57 53	13.95	0.89	1.42		
12	11 06 27.7	−77 35 54	13.26	1.10	1.65		
13	11 06 39.3	−77 36 04	12.40	1.23	1.78	ISO-ChaI 79	1
14	11 06 40.1	−76 48 35	12.48	0.94	1.03		
15	11 07 06.5	−76 37 17	10.22	1.50	0.93		
16	11 07 18.8	−77 31 56	12.63	1.93	1.49		
17	11 07 27.9	−76 48 35	13.91	0.74	0.38		
18	11 07 46.9	−76 15 17	12.22	0.71	0.94		
19	11 07 50.0	−77 38 07	13.50	1.55	2.23		
20	11 08 20.6	−76 26 49	13.80	0.67	0.62		

Table 3—Continued

Star	α(2000.0)	δ(2000.0)	K	$H-K$	$J-H$	Id.	Ref.
21	11 08 22.6	−76 49 19	12.32	1.12	0.82		
22	11 08 41.9	−77 13 22	13.78	1.47	0.83		
23	11 08 42.9	−77 10 08	12.85	0.95	0.92		
24	11 08 44.5	−76 13 29	12.92	0.79	0.56		
25	11 09 29.4	−76 34 46	13.68	0.95	1.35	NIR-14	2
26	11 09 32.3	−76 30 17	13.00	0.94	1.16		
27	11 09 33.9	−77 53 33	13.90	0.82	1.19		
28	11 09 50.7	−78 04 19	13.80	0.77	1.07		
29	11 09 52.0	−76 39 12	11.67	0.69	1.02	ISO-ChaI 217	1
30	11 09 53.4	−77 28 36	12.48	0.85	1.24	ISO-ChaI 220	1
31	11 09 54.1	−76 31 11	12.75	0.98	1.11	ISO-ChaI 225	1
32	11 10 01.6	−77 47 47	13.97	1.23	1.46		
33	11 10 04.5	−77 48 22	13.65	1.21	1.42		
34	11 10 06.2	−76 40 20	13.85	1.06	1.53		
35	11 10 16.8	−77 43 44	13.01	1.38	1.28		
36	11 10 47.6	−76 32 38	13.22	0.84	0.24		
37	11 10 49.4	−76 38 08	13.87	1.19	0.76		
38	11 10 53.2	−76 16 53	13.96	0.78	0.18		
39	11 10 56.9	−77 13 26	13.93	0.77	1.03		
40	11 10 58.2	−76 17 56	13.82	0.77	0.93		

Table 3—Continued

Star	α(2000.0)	δ(2000.0)	K	$H-K$	$J-H$	Id.	Ref.
41	11 11 08.9	−76 49 12	13.21	0.95	1.54		
42	11 11 21.1	−78 05 20	13.25	0.69	0.64		
43	11 11 27.8	−76 50 17	13.48	0.90	1.09		
44	11 11 35.7	−76 53 26	13.19	1.16	1.79		
45	11 11 42.6	−78 05 21	13.88	0.66	0.53		
46	11 11 48.7	−76 12 21	13.83	0.75	0.49		
47	11 11 54.5	−76 58 29	13.71	1.29	0.98		
48	11 11 57.5	−77 21 57	13.72	1.38	1.13		
49	11 12 03.7	−76 51 33	13.51	1.27	1.82		
50	11 13 25.3	−77 00 23	11.55	0.98	0.67		
51	11 13 26.0	−77 00 32	12.40	1.20	0.28		
52	11 13 42.7	−77 55 30	13.71	0.45	0.25		
53	11 14 31.4	−78 06 44	13.03	0.98	0.75		
54	11 14 23.6	−77 56 12	13.73	0.84	0.80		
55	11 16 13.2	−77 25 15	11.00	0.85	0.21		
56	11 18 09.0	−78 14 11	13.71	1.03	0.72		

Note. — Units of right ascension are hours, minutes, and seconds, and units of declination are degrees, arcminutes, and arcseconds.

References. — (1) Persi et al. (2000), (2) Oasa et al. (1999)

Table 4. Candidate Pre-Main Sequence Stars with $K > 14.0$.

Star	$\alpha(2000.0)$	$\delta(2000.0)$	K	$H-K$	$J-H$	Id.	Ref.
57	10 40 47.6	−77 36 49	15.12	0.95	0.73		
58	11 04 17.1	−77 25 49	15.34	0.86	0.65		
59	11 04 27.0	−77 28 02	14.87	1.14	1.02		
60	11 04 30.5	−77 34 41	14.33	0.96	0.89		
61	11 04 32.0	−77 54 09	15.27	1.02	0.88		
62	11 04 35.8	−77 29 09	15.34	0.99	0.94		
63	11 04 36.2	−77 50 12	14.76	1.21	1.26		
64	11 04 38.7	−77 24 21	14.49	1.27	0.87		
65	11 04 39.1	−77 40 05	14.39	1.56	1.18		
66	11 04 48.4	−77 49 20	15.45	1.69	0.85		
67	11 05 37.0	−76 51 18	15.33	1.48	1.04		
68	11 05 41.2	−76 38 38	15.12	0.91	0.58		
69	11 05 42.6	−77 26 30	14.33	2.09	2.67		
70	11 05 43.0	−77 31 58	14.43	1.46	1.16		
71	11 06 33.5	−77 52 26	14.79	0.98	0.74		
72	11 06 35.3	−77 21 10	15.94	1.20	0.95		
73	11 06 49.4	−77 34 37	14.99	1.51	1.78		
74	11 06 51.0	−77 11 33	15.08	1.16	0.64		
75	11 06 54.5	−77 25 54	15.30	1.36	0.70		
76	11 06 59.6	−77 18 29	14.90	1.59	1.52		

Table 4—Continued

Star	α(2000.0)	δ(2000.0)	K	$H-K$	$J-H$	Id.	Ref.
77	11 07 59.0	−78 00 13	15.05	1.41	0.84		
78	11 08 27.3	−77 47 20	14.75	1.44	0.93		
79	11 08 51.6	−77 02 30	14.82	1.75	0.65		
80	11 08 51.5	−77 06 44	15.10	0.87	0.64		
81	11 09 08.3	−78 14 25	15.09	1.31	0.69		
82	11 09 18.8	−77 39 37	15.10	1.26	1.10		
83	11 09 24.1	−76 34 55	14.87	1.46	1.56	NIR-11	2
84	11 09 24.7	−78 13 54	15.69	0.86	0.78		
85	11 09 52.7	−77 49 08	14.87	1.80	1.37		
86	11 10 01.7	−77 19 20	15.35	1.05	1.00		
87	11 10 04.3	−77 27 15	15.34	2.01	0.66		
88	11 10 17.7	−77 22 18	15.69	1.31	1.03		
89	11 10 19.6	−77 11 20	14.57	0.94	0.89		
90	11 10 24.6	−77 23 06	15.58	1.93	0.73		
91	11 10 26.2	−76 44 09	15.99	1.18	0.60		
92	11 10 29.4	−76 31 12	15.36	1.37	0.58		
93	11 10 29.8	−77 21 12	15.11	1.43	0.64		
94	11 10 37.9	−77 01 39	15.29	1.21	0.75		
95	11 10 39.2	−77 02 48	15.44	1.45	1.10		
96	11 10 46.1	−77 17 07	14.47	0.99	0.88		

Table 4—Continued

Star	α(2000.0)	δ(2000.0)	K	$H-K$	$J-H$	Id.	Ref.
97[a]	11 11 06.3	−78 03 57	14.74	1.00	0.98		
98	11 11 11.5	−76 44 37	15.02	1.24	1.21		
99	11 11 12.3	−76 47 51	15.28	1.01	0.99		
100[a]	11 11 15.6	−78 13 22	14.71	1.28	0.87		
101	11 11 21.3	−77 24 15	15.02	0.97	0.80		
102	11 11 28.6	−78 05 28	15.02	1.61	1.03		
103	11 11 30.2	−78 10 10	15.06	0.89	0.72		
104	11 11 34.3	−76 47 35	15.34	0.82	0.67		
105	11 11 47.3	−77 08 12	14.50	1.40	1.00		
106	11 11 48.1	−77 25 46	15.06	0.95	0.81		
107	11 12 05.1	−77 29 58	15.22	1.17	1.16		
108	11 12 13.1	−77 22 37	14.47	1.07	1.02		
109	11 13 02.6	−77 22 08	14.72	1.13	0.74		
110	11 13 23.8	−77 25 28	15.64	1.55	1.55		
111	11 13 53.1	−77 37 01	14.62	1.93	1.91		
112[a]	11 13 56.0	−77 06 35	14.28	1.13	0.72		
113	11 14 17.3	−76 48 18	15.11	0.95	0.86		
114	11 15 00.3	−78 03 13	15.04	0.96	0.89		
115	11 16 30.3	−78 05 08	15.30	1.12	0.77		
116	11 16 46.0	−77 37 40	15.06	0.89	0.74		

Table 4—Continued

Star	α(2000.0)	δ(2000.0)	K	$H-K$	$J-H$	Id.	Ref.
117	11 17 36.8	−77 45 35	15.18	1.03	0.68		
118	11 18 02.2	−77 41 30	15.61	0.86	0.58		

Note. — Units of right ascension are hours, minutes, and seconds, and units of declination are degrees, arcminutes, and arcseconds.

[a]Star with fuzzy image at K.

References. — (1) Persi et al. (2000), (2) Oasa et al. (1999)

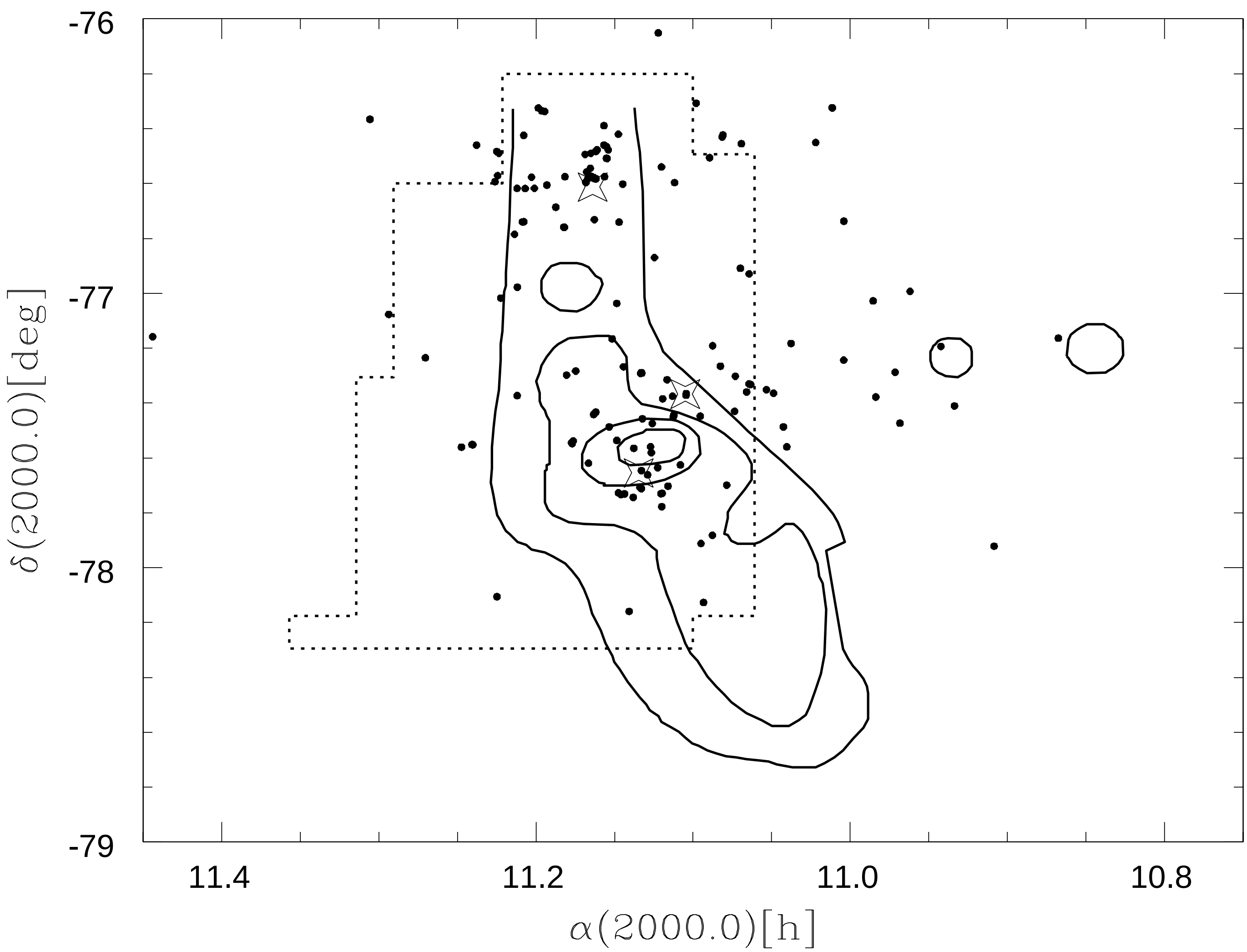

-76
-77
-78
-79
11.4
11.2
11.0
10.8
δ(2000.0)[deg]
α(2000.0)[h]

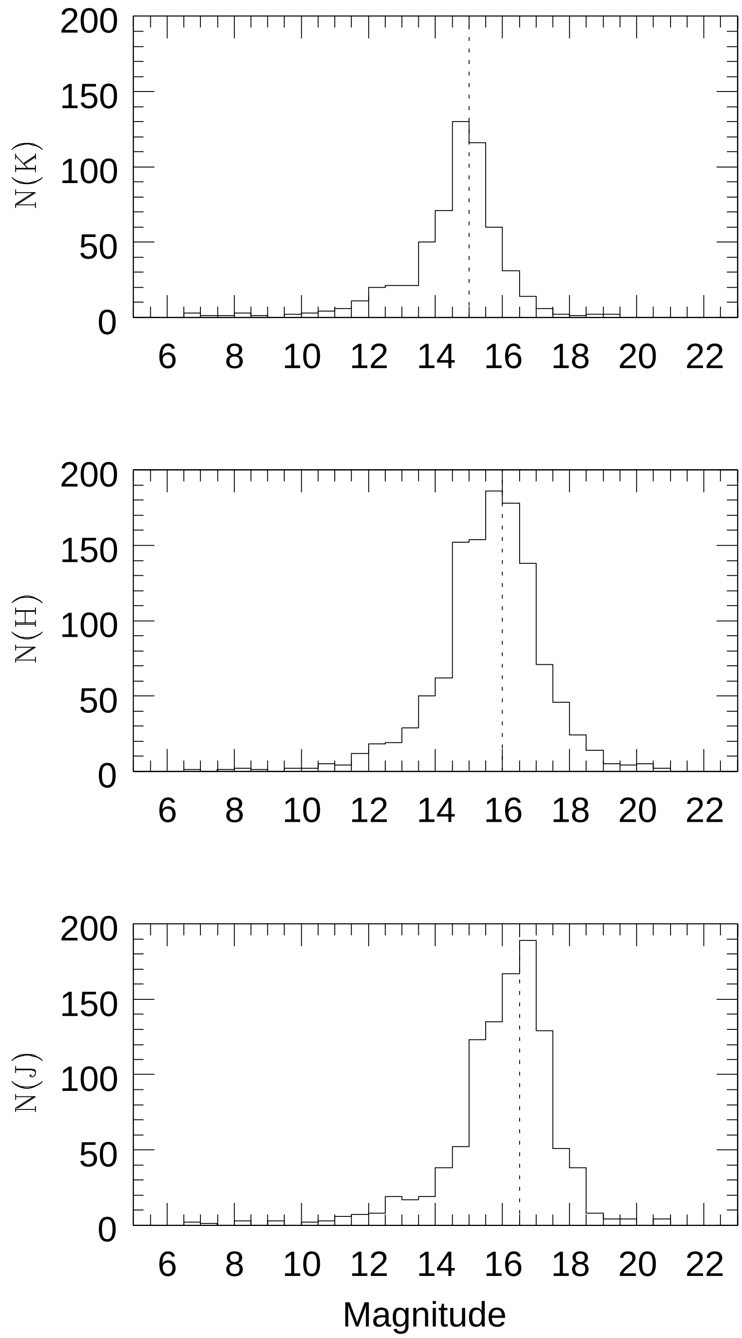
N(K)
N(H)
N(J)
0
50
100
150
200
6
8
10
12
14
16
18
20
22
Magnitude

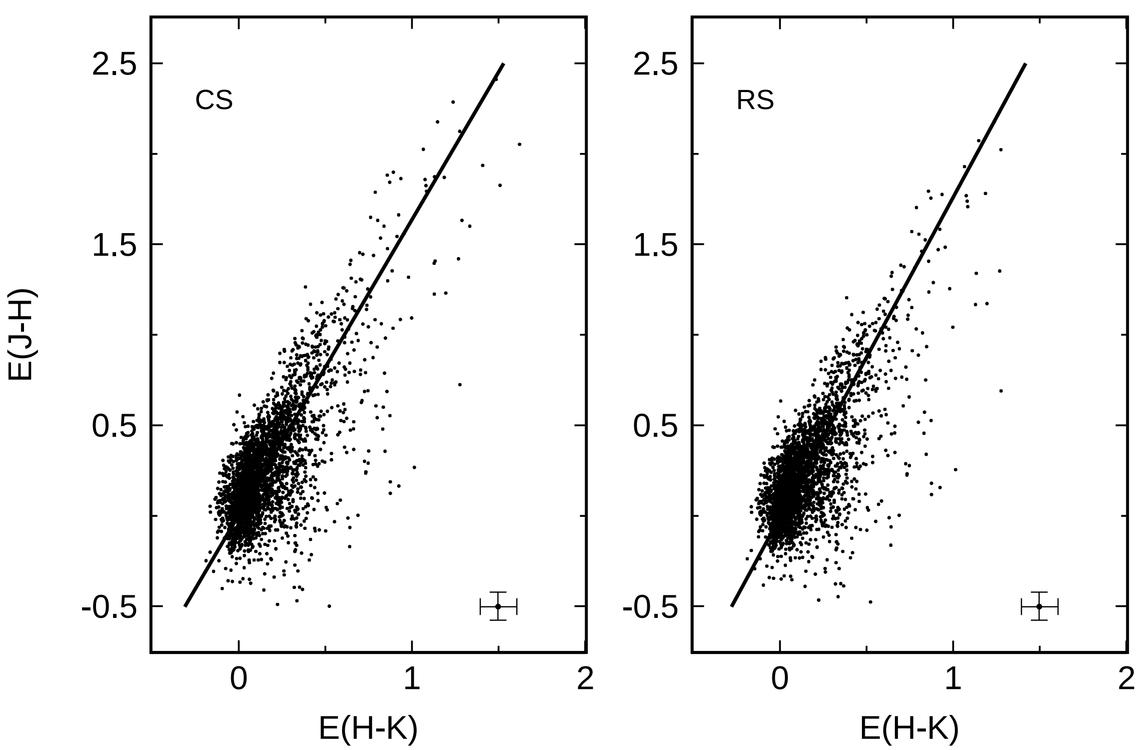
CS
RS
E(J-H)
E(H-K)
E(H-K)
2.5
1.5
0.5
-0.5
2.5
1.5
0.5
-0.5
0
1
2
0
1
2

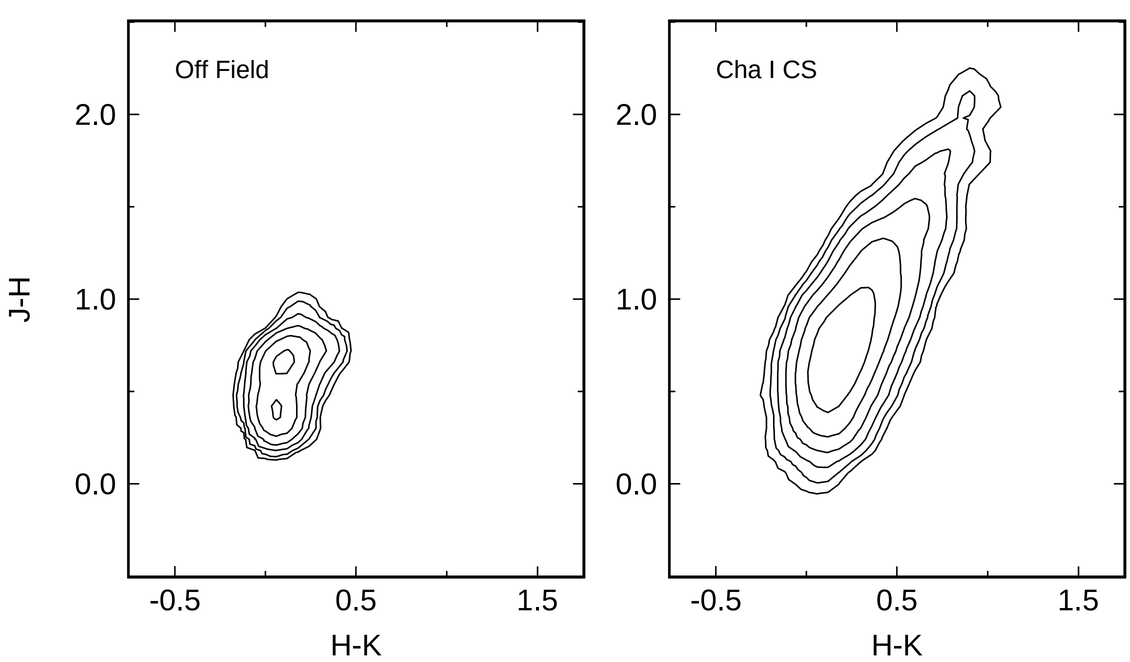

Off Field
Cha I CS
2.0
1.0
0.0
J-H
-0.5
0.5
1.5
H-K

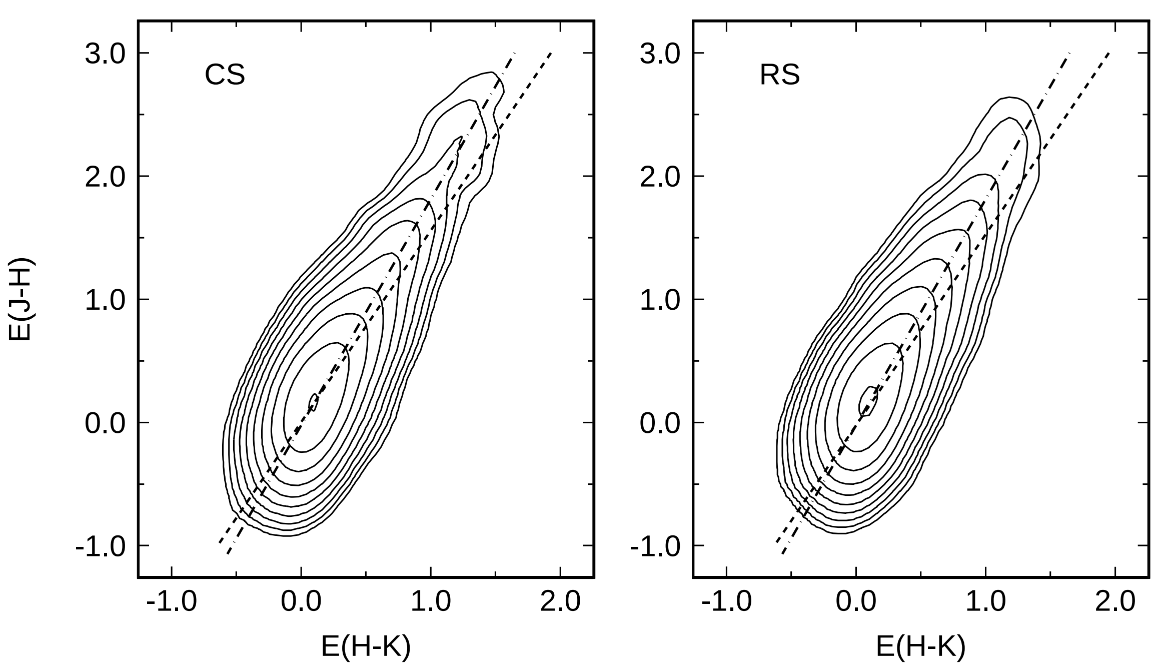
CS
RS
E(J-H)
E(H-K)
E(H-K)
3.0
2.0
1.0
0.0
-1.0
-1.0
0.0
1.0
2.0

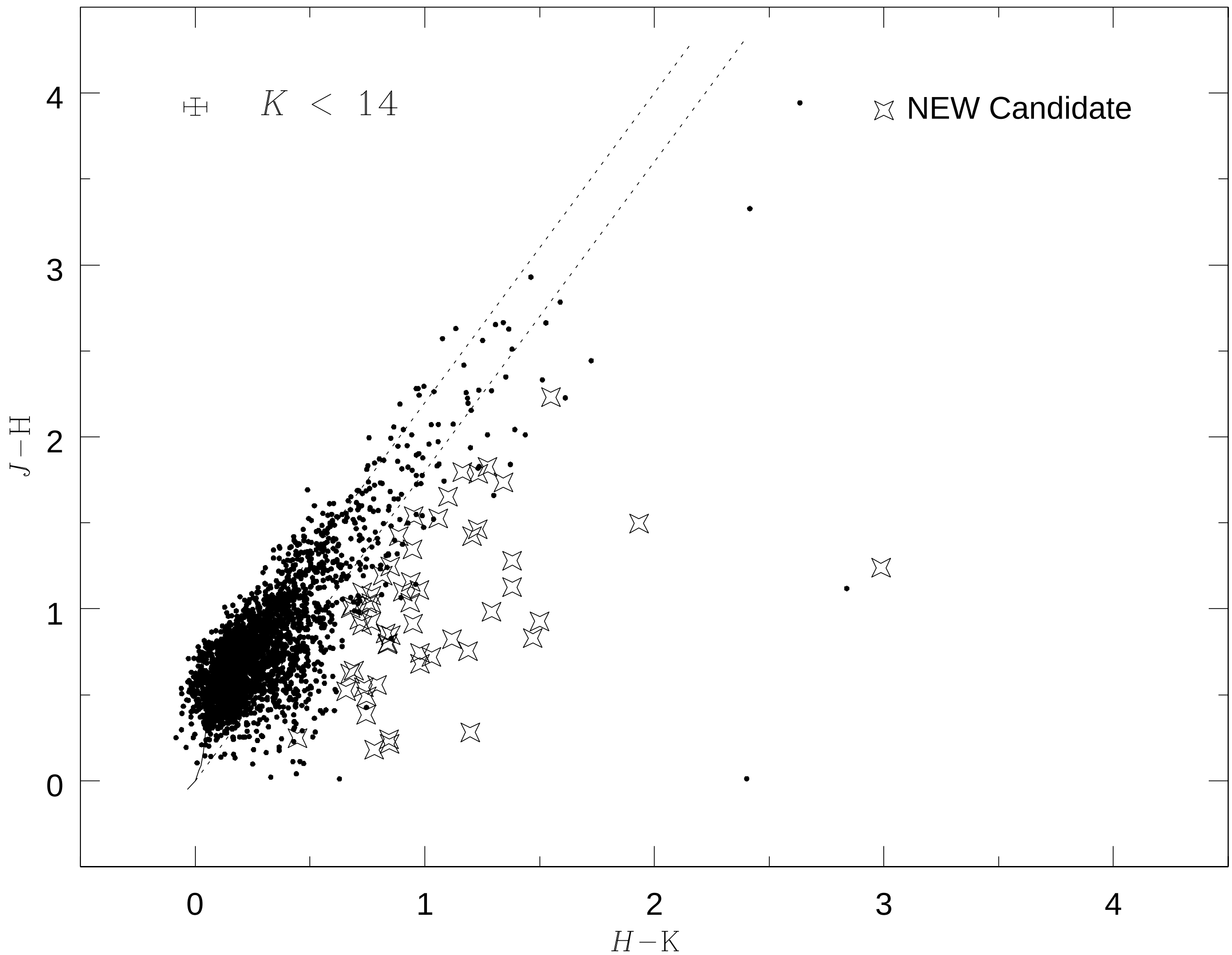
K < 14
NEW Candidate
J − H
H − K
0
1
2
3
4
0
1
2
3
4

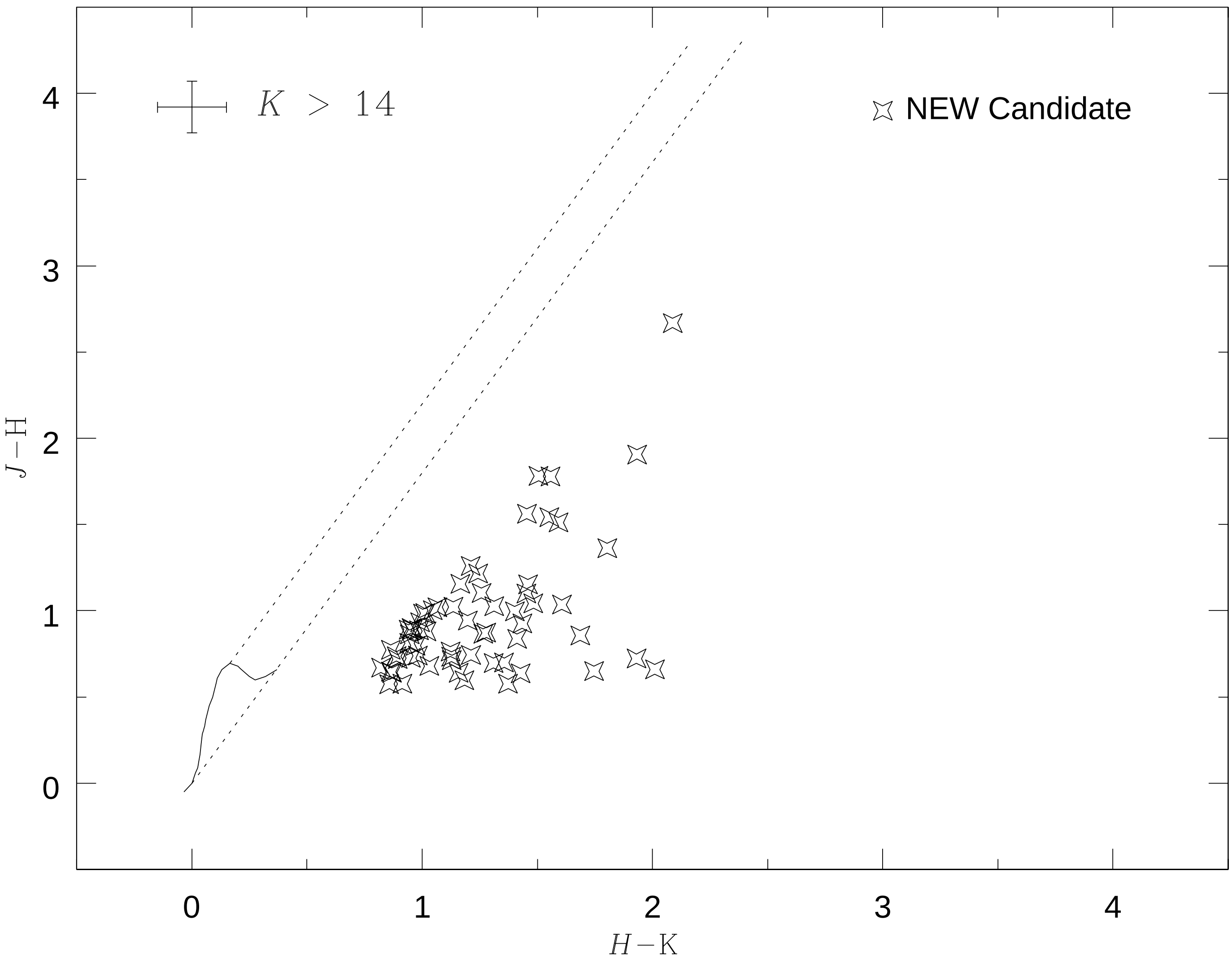

$K > 14$
NEW Candidate
0
1
2
3
4
$J-\mathrm{H}$
$H-\mathrm{K}$

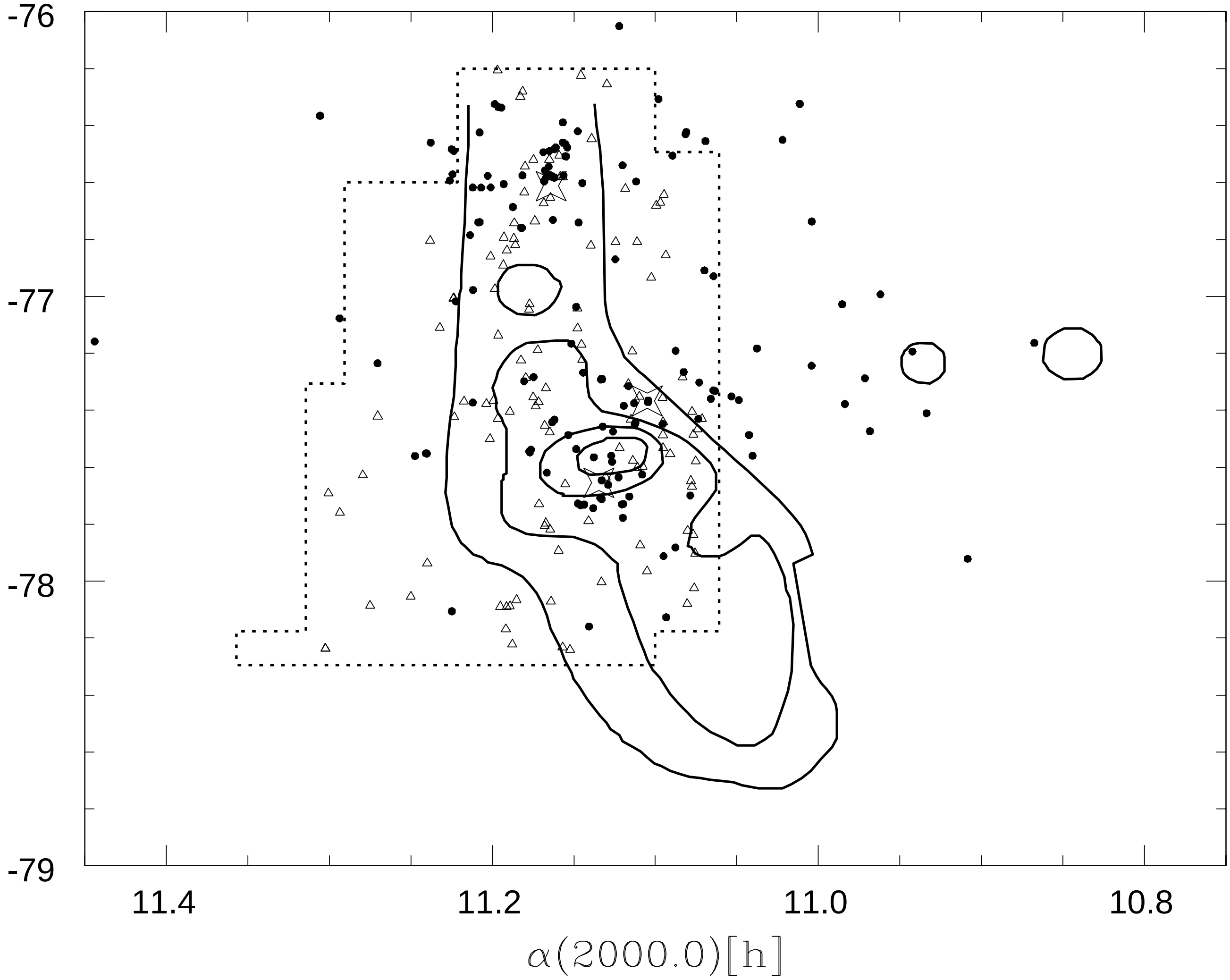

-76
-77
-78
-79
11.4
11.2
11.0
10.8
δ(2000.0)[deg]
α(2000.0)[h]